Modelling of form in thermotropic polymers†

By A. H. Windle, H. E. Assender and M. S. Lavine

*Department of Materials Science and Metallurgy, Pembroke Street,
Cambridge CB2 3QZ, U.K.*

A lattice model of liquid crystalline microstructure has been developed. It provides the basis for the three-dimensional solution of the Frank elasticity equations for given boundary conditions while, in addition, providing a mechanistic representation of the development of texture as the microstructure relaxes with time. It is also able to represent disclination motion and the processes associated with their interaction. In particular, it has been used to study $(s = \pm\frac{1}{2})$ disclination loops, both those described by a single rotation vector, Ω, and those in which Ω has a constant angular relationship with the loop line and are equivalent to a point singularity at a distance much larger than the loop radius. The application of the model to disclinations of unit strength, which are unstable both energetically and topologically, has shown that the decomposition into two $\frac{1}{2}$ strength lines of lower total energy occurs much more readily than topological escape in the third dimension. The implication for structures observed in capillary tubes is discussed. The influence on microstructure of a splay constant much higher than that of twist or bend is explored in the context of main-chain liquid crystalline polymers, in particular, the stabilization of tangential +1 lines under such conditions is predicted in accord with observed microstructural features.

1. Background

The study of liquid crystals is a mature science. For over 100 years the light microscope has been the primary tool for the observation of microstructural form in these materials. The literature abounds with the rich variety of textures which have been reported. The analysis of microstructure stems from Lehmann (1904), who first described a Schlieren texture and drew director maps of what we now call disclinations. Friedel (1922) provided the modern framework of structural understanding and much of the accepted nomenclature, while Zocher (1929) laid the basis for disclination analysis in liquid crystals which was extended and refined by Frank (1958). More recently Kléman (1983) has interfaced the geometric understanding to algebraic topology. It is perhaps surprising that an area which has attracted such quality attention over so many years should still be of interest. However, the recognition within the last two decades of liquid crystallinity as a state of matter in synthetic polymers, has involved the identification of a number of new textures, some fine scale and very difficult to interpret, others such as the banded textures, quite striking. The purpose of the work described in this paper

---

† This paper was produced from the authors' disk by using the TEX typesetting system.

© 1994 The Royal Society

is, through the device of microstructural modelling, to reinforce our geometric appreciation of disclination organization in three dimensions, and to do this in a way which can simulate the evolution of microstructures and, eventually, their response to complex boundary conditions and applied fields.

While the new structures seen in polymeric liquid crystals may be challenging to interpret, there is a distinct experimental advantage with these materials. The observation of textures in small-molecule mesophases is straightforward in the case of light microscopy of thin films contained between slides. However, it is not generally possible to quench-in the liquid structure, for when solidification occurs by virtue of crystallization, the structure is largely 'rewritten' as the crystals form. On the other hand, in main-chain thermotropic materials, such as those based on random copolymers, the limited crystallization which does occur (about 20%) does not appear to affect significantly the structure which subsequently freezes to a glass at T_g. Hence, the microstructural form of the frozen melt may be investigated for bulk specimens in which the influence of the boundary conditions is minimal. Fractography is often rewarding. Figure 1a shows the local structure in a sample of thermotropic copolyester as revealed on the fracture surface. The material is fissile, with the easy direction of fracture corresponding to the local chain axis. Further confirmation of this relationship can be achieved by lightly etching the fracture surface which reveals the crystals as cross striations. The platelet form of the crystals and the fact that their thin axis corresponds to the chain axis have been confirmed by electron microscopy (Spontak & Windle 1990; Hanna *et al.* 1992). Figure 1b is a fractograph of a banded structure; the shear axis is horizontal and observation in transmitted polarized light would reveal parallel bands normal to this axis. Thin sections of a bulk sample can also be prepared by grinding and polishing methods familiar to petrologists. While it is important to remain wary of any influence of crystallization on the details of the quenched melt structure, we are confident from both the appearance of the structures, and the measurements of similar orientation functions for the crystalline and liquid crystalline components of the diffraction pattern, that rapid cooling enables one to observe an accurate solid replica of the liquid crystalline melt.

2. The lattice model

The initial stages of development of the lattice model for liquid crystalline microstructure has been described in earlier publications (Bedford *et al.* 1991; Bedford & Windle 1993). The model bears some relationship to that of Kilian & Hess (1989, 1990) and of earlier Monte Carlo based molecular scale modelling of Lebwohl & Lasher (1972). The model is summarized in figure 2. It consists of a cubic array of cells, each of which is assigned a director orientation (figure 2a). The scale of the model is such that each cell contains many molecules and is characterized by a director defining their common orientation. In the case of the work reported here, the local molecular distribution is assumed to be uniaxial, although biaxial systems are possible and potentially treatable with models of this type. The algorithm is outlined in figure 2b. Starting conditions are either random, the director of each cell being set in a random orientation with either free, fixed or periodic boundary conditions, or correspond to a particular arrangement which is written into the model before commencement of relaxation. A cell is

Figure 1. (*a*) Fracture surface revealing the local director orientation in a sample which would show a schlieren texture in transmitted polarized light. Material: random copolymer of 75% hydroxybenzoic acid and 25% hydroxynaphthoic acid. $M_W = 5800$. Courtesy, Dr A. Anwer. (*b*) Fracture surface through a thin sample of the same polymer as in (*a*). It has been sheared and quenched and shows a banded texture in transmitted polarized light. The fracture plane is parallel to the shear plane and the shear direction is horizontal. Courtesy, Dr T. J. Lemmon.
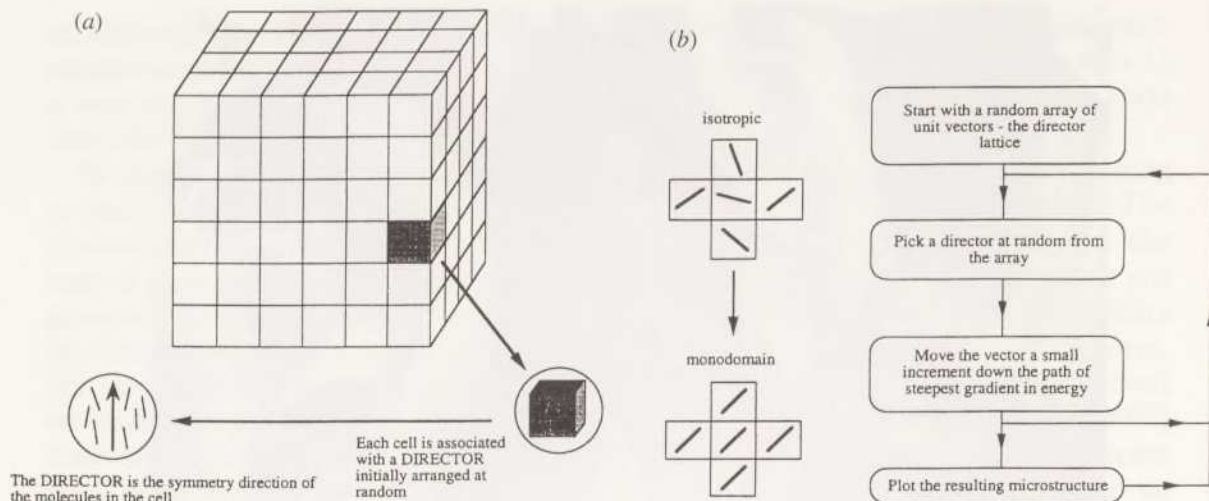
Figure 2. (a) The lattice model. Each cell is characterized by a director, and is taken to be much larger than molecular dimensions. (b) The algorithm used. Each cell is visited at random, and the orientation of its director changed on a path with will reduce its energy with respect to the orientation of the directors of the six nearest neighbour cells.

selected at random and its energy calculated by summing the individual energy contributions due to the orientational distortion between it and each of its six (in three dimensions) nearest neighbours. The orientation of the central vector is then changed by a small amount, one degree or less, down the path of steepest energy gradient. Another cell in the model is then chosen at random and the process repeated, and so on. The evolving model texture is printed out as required.

The energy function which has been found to be most successful is $\sin^2(\Delta\phi)$. The reasons for preference of this harmonic function have been discussed (Assender & Windle 1994). In summary, it has the following attributes:

1. It approximates to $E \propto \Delta\phi^2$ at low angles, which is the assumption of the Frank equation for elastic energy.

2. The summation of six energy functions corresponding to the surrounding cells corresponds to the summation of six harmonic functions differing in phase and amplitude. The consequence is thus another harmonic function, sketched in terms of Euler angles in figure 3. It has the advantage of a single minimum, so that gradients at all points on the energy surface lead to this minimum.

3. The lattice is invisible. This means that a symmetrical field, as would for example surround the centre of a singularity, would lead to a completely flat energy–orientation relationship for the central director irrespective of the relative orientation of the disclination and the lattice.

Figure 4 illustrates the model relaxing in three dimensions. It is a series of sections (on the same plane) taken after the model had run after various increasing intervals. The degree to which a director is angled out of the plane is illustrated by shortening its length, so that directors exactly normal to the section appear as points. The relaxation sequence can be followed as small regions sharing common orientation appear in (b) with many $\frac{1}{2}$ strength disclinations identifiable. Relaxation continues through the apparent annihilation of defects of opposite sign, although in three dimensions this may simply be the result of a disclination loop moving out of the chosen section. The movement of disclinations was not
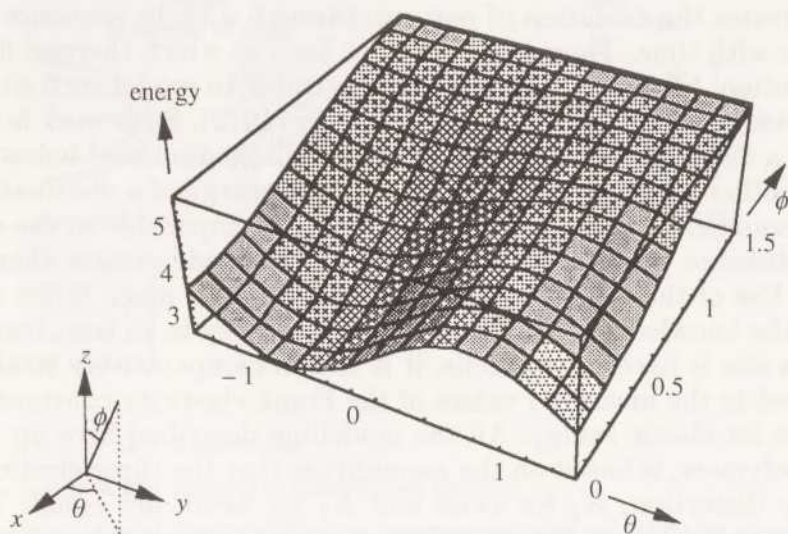
Figure 3. The energy of a director as a function of its orientation expressed as Euler angles obtained using the $\sin^2 \Delta\phi$ function. The six nearest neighbour cells have directors chosen at random. The energy surface has only a single minimum and tessellates in θ and 2ϕ.
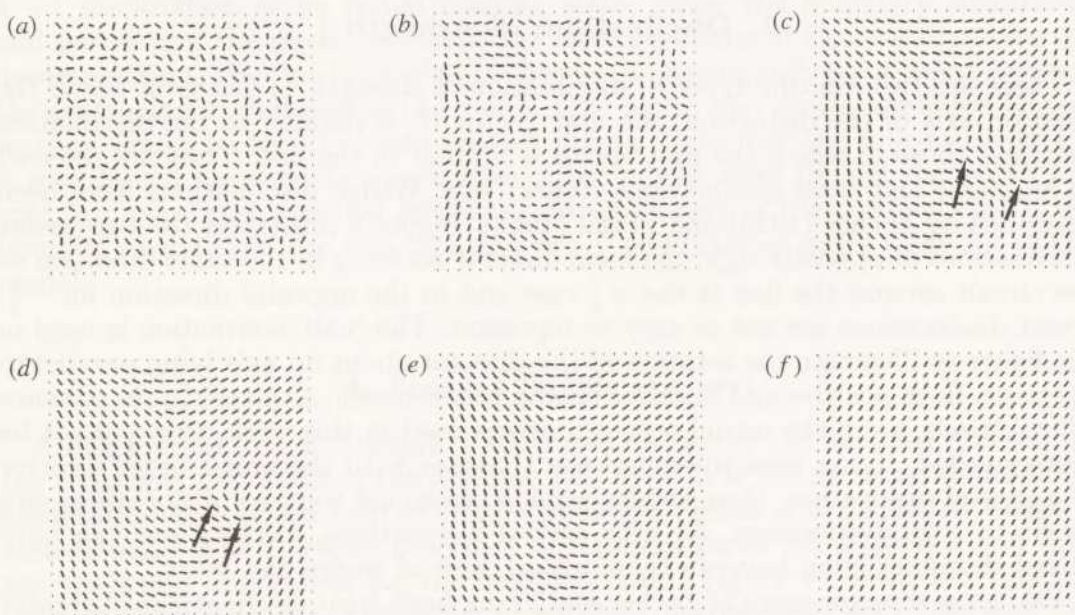

Figure 4. A central section through an equiaxial three-dimensional lattice model of 15 625 cells. The pattern of directors in the section evolves as the model relaxes. The dots around the outside signify free boundary conditions. Directors are drawn as shorter projections as they increasingly tilt out of the plane. The number of iterations per cell were: (a) initial condition, (b) 33, (c) 164, (d) 247, (e) 329 and (f) 1973. Note the elimination of a $\pm\frac{1}{2}$ pair marked by arrows.

achieved by Kilian & Hess in their model, at least in the absence of any external field (Kilian & Hess 1990). The sequence is completed as a monodomain with orientation unrelated to the lattice.

The questions arises as to the scaling of the model with respect to size, energy and time. The model operates without assignment of quantities to any of these.

It thus illustrates the evolution of pattern, through a cyclic sequence which may not be linear with time. There is a small size limit at which thermal fluctuations, brownian motion, becomes significant. It is possible to model such situations following the pioneering work of Lebwohl & Lasher (1972). Such work is in progress, but it is not a feature of this paper. In fact, as will be discussed below, the model does have another size constraint in that the true energy of a disclination line can only be determined by a model with a resolution comparable to the diameter of the core, a distance perhaps only an order of magnitude greater than molecular dimensions. Use of the model to represent structures on much larger scales must be made in the knowledge that disclination core energy is, in fact, being underestimated. If a size is fixed for the cells, it is then a comparatively straightforward matter to feed in the measured values of the Frank elasticity constants to obtain actual values for elastic energy. All the modelling described here up to the final section on polymers, is based on the assumption that the three elastic constants, K_1 for splay distortion, K_2 for twist and K_3 for bend, are equal. The matter of linearity with time, and the modelling of actual rates of relaxation remains a future objective. It will require knowledge of rotational viscosities of the medium, and expression of the energy gradients as torques.

3. Disclinations of strength $\frac{1}{2}$

There are two limiting types of disclination of strength $\frac{1}{2}$. Those in which the rotation axis of the distortion, the unit vector Ω, is parallel to the disclination line, and those in which the unit vector is normal to the line. They are referred to as *wedge* and *twist* disclinations respectively. Wedge disclinations have been described by Zocher (1929) and Frank (1958). Figure 5 illustrates the two wedge disclinations of opposite sign, the local director rotating in the same direction as the circuit around the line in the $+\frac{1}{2}$ case and in the opposite direction for $-\frac{1}{2}$. Twist disclinations are not as easy to represent. The 'nail' convention is used in the figure to illustrate the rotation of the director about an axis lying parallel to the page. Both positive and negative examples are shown, although in the absence of nail heads, as in the model representations used in this work, they cannot be distinguished. If one were to equate the Ω vector with the unit Burger's vector of a crystal dislocation, then wedges would correspond to screw dislocations and twists to edge dislocations. As with crystal dislocations, disclinations can have mixed character lying between the limiting cases of wedge and twist.

While the director maps of Zocher and Frank both treat disclinations of greater strength than $\frac{1}{2}$, such higher order line singularities need to be kept in perspective in that they are intrinsically unstable. It is well known (Frank 1958) that the energy of a disclination (E) is proportional to the strength (s) squared. A disclination of strength unity, for example, will undergo the dissociation reaction:

$$s_{+1} \rightarrow s_{+1/2} + s_{+1/2}, \qquad E \rightarrow \tfrac{1}{4}E + \tfrac{1}{4}E = \tfrac{1}{2}E.$$

This reaction can be viewed as a dissociation of the $+1$ disclination followed by the elastic repulsion of the two $\frac{1}{2}$s of like sign. Meyer (1973) pointed out that the many observations of disclinations of integral strength, particularly ± 1, from microstructural observations in fact represented point singularities of unit strength at the sample surfaces.
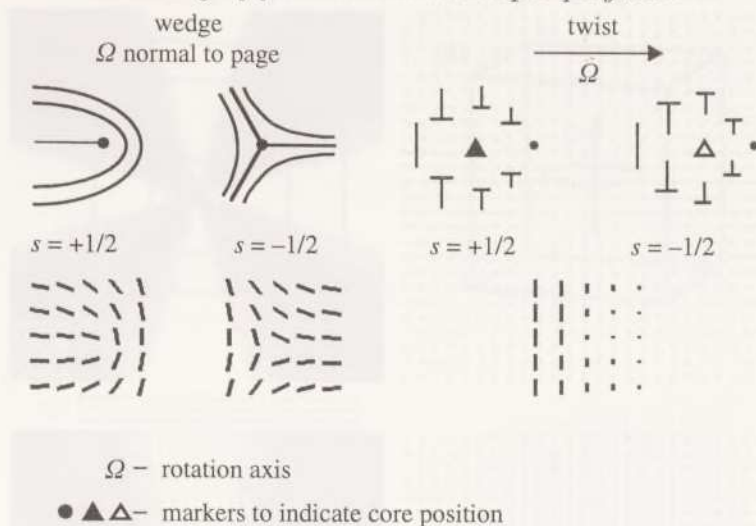
Figure 5. Diagram showing the local director pattern surrounding examples of pure wedge and twist disclinations of strengths $+\frac{1}{2}$ and $-\frac{1}{2}$.

Dissociation behaviour has been modelled in two dimensions by setting up a $+1$ disclination as an initial starting state, fixing the boundary conditions, and permitting the model to relax. The model sections in figure 6 illustrate the decomposition. The two $\frac{1}{2}$s repel until they are approximately equidistant between the centre and extremities of the model. The figure also shows simulated images as they would be seen between crossed polars. Note how the four-brush image is maintained towards the extremities of the model, even though the centre has split into two-brush contrast patterns centred on each of the disclinations. If the boundary conditions are free then the two $\frac{1}{2}$ disclinations move right out of the model.

4. Loops I (single Ω class)

A disclination line of strength $\frac{1}{2}$ separates regions of the material differing in the rotational distortion of the director field by π. It is instructional to draw the disclination as a closed loop so that it bounds a region of π distortion within a monodomain. The Ω vector describes the orientation of the distortion and thus has the same orientation for the complete loop. Figure 7 shows two limiting cases of single Ω loops. Figure 7a, in which Ω lies parallel to the plane of the loop, 7b in which it is normal to the loop. In the first case the character of the loop changes as the line curves from being parallel to Ω, to being perpendicular, back to parallel and so on. This transition in character for constant Ω was first pointed out by Bouligand *et al.* (1973), although it is a familiar property of a glissile dislocation loop in a crystal. There are four positions on the loop at which the disclination is either pure wedge or pure twist as marked, but in general it is of mixed character. We refer to the loop as a wedge–twist loop. Figure 7c shows diametric cross sections through such a loop, one normal to Ω showing cross section through the pure wedge parts of the loop, $+\frac{1}{2}$ on the left, $-\frac{1}{2}$ on the right, the other showing the twist parts which again will be of opposite sign although the absence of nail heads on the diagram makes this less than obvious.
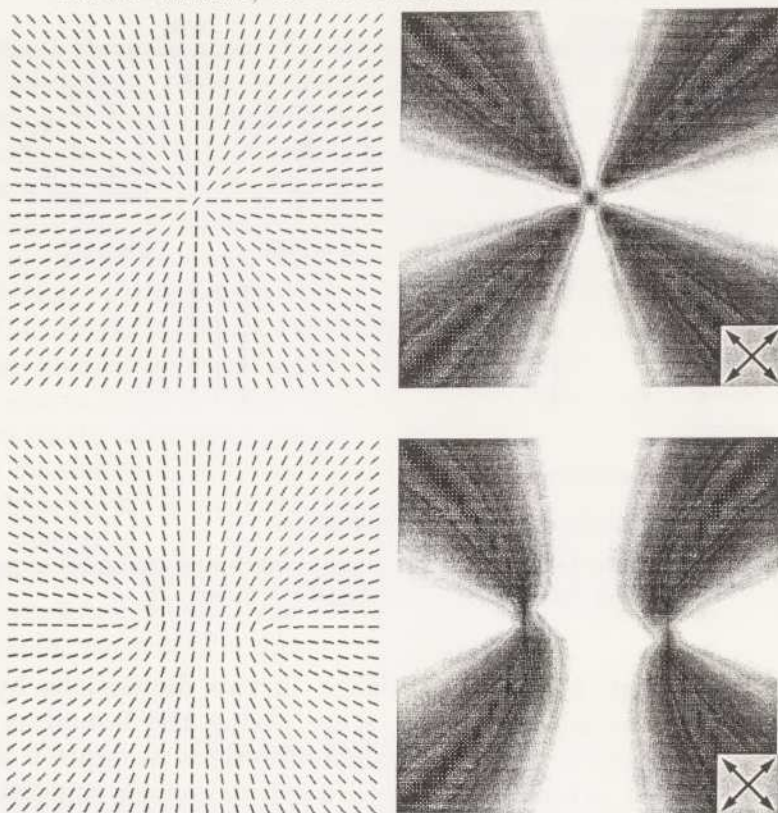
Figure 6. Diagrams of a two-dimensional model in which all the directors are held within the single plane. The +1 disclination is set up as the initial condition. As the model runs to simulate relaxation with fixed boundary conditions, the disclination decomposes into two disclinations of strength $+\frac{1}{2}$ which move apart under their mutual repulsion until reaching an equilibrium position after 1890 iterations per cell. The simulated optical micrographs are by courtesy of J. Hobdell.

The director field of the 'wedge' section has been described as a 'pincement'. The second limiting case in which Ω is normal to the plane of the loop bounds a region of twist distortion. As Ω is normal to the line at all points, the disclination has twist character at all points, and the loop is referred to as a twist loop. Two orthogonal cross sections of a twist loop are shown in figure 7d.

A significant aspect of these class I loops is that their expansion provides a mechanism for the propagation of rotational distortion within the material, perhaps under the influence of the rotational component of a simple shear field. The corollary to this statement is that the loops, if permitted to relax, will collapse and self annihilate as the diametrically opposed components which have opposite sign all meet at the centre. Figure 8 is a model relaxation sequence showing the collapse of a wedge–twist loop (in wedge cross section). The driving force for this collapse has two components: the elimination of the distorted material bounded by the loop which could also be expressed as an attraction between the components of the loop of opposite sign; and the reduction in the length of the loop itself, which in an analogous sense to dislocations, can be expressed as a line tension.

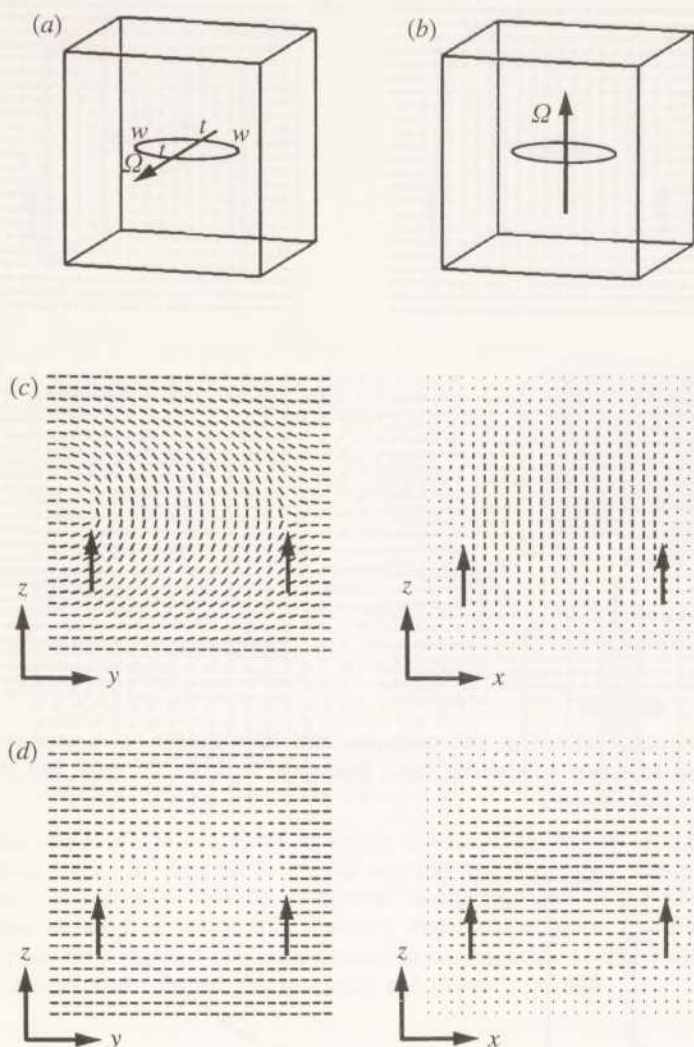The twist loop collapsed and was eliminated in the same way.

Figure 7. Representation of $s = \frac{1}{2}$ disclination loops which are defined by a single rotation vector, Ω. (*a*) Sketch of limiting case in which Ω is in the plane of the loop which has wedge-twist character. (*b*) Loop of case in which Ω is normal to the plane of the loop which is entirely a twist disclination. (*c*) Two orthogonal sections through a model of a wedge-twist loop. Each section is normal to the plane of the loop. (*d*) Two sections, equivalent to those of (*c*), but in this case through a twist loop.

The energy per unit length (E/L) of a disclination can be expressed as

$$E/L = \pi K s^2 (\ln(R/r_c) + 0.5),$$

where K is the Frank constant (assuming $K_1 = K_2 = K_3$), R the radius of the surrounding volume of material deemed to be associated with the line under consideration and r_c the core radius. The value of 0.5 for the core energy, while derived by setting the energy of the material in the core volume equal to the energy density at the radius r_c bounding the core, is not often quoted as such. Meyer (1973) would appear to choose $1/\pi$, whereas Cladis (1974) takes it to be unity.

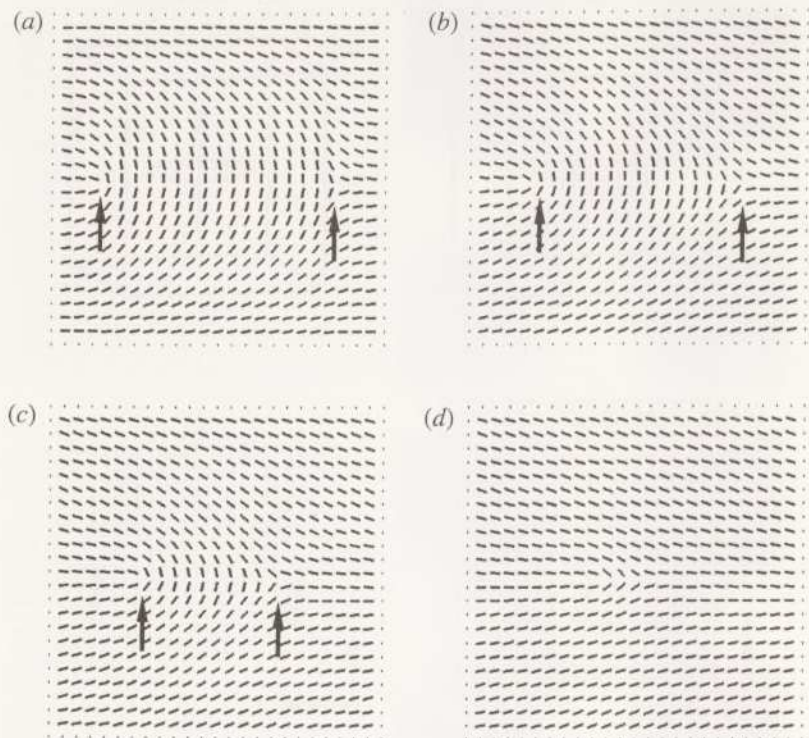For a loop we take the upper limit of integration about the line, R, to be the

Figure 8. Model sequence showing the collapse and elimination of a wedge-twist loop. The diagrams correspond to equal modelling time intervals: 0, 115, 230 and 345 iterations per cell respectively.
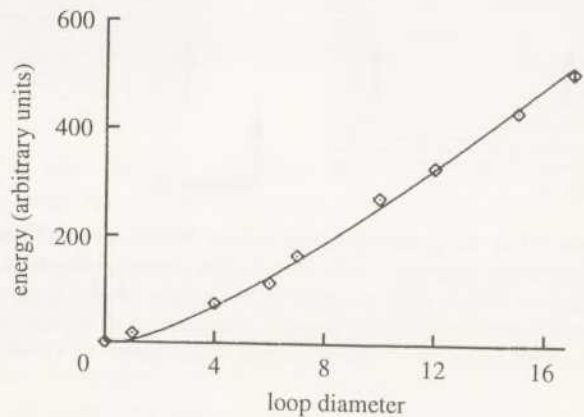

Figure 9. Energy values for a collapsing wedge-twist loop determined from the model. The energy units are arbitrary and the loop diameter is expressed in model cell units. The continuous curve is determined from the loop energy equation, assuming a core diameter of one cell, and scaled vertically to fit the model points.

radius of the loop R_l. Then

$$E_l = 2\pi^2 K s^2 R_l (\ln(R_l/r_c) + 0.5).$$

Figure 9 shows a plot of the energy of the model, in arbitrary units, as a function of the loop diameter expressed as cells. The continuous plot is the calculated energy of the loop from the equation above taking the diameter of the core to
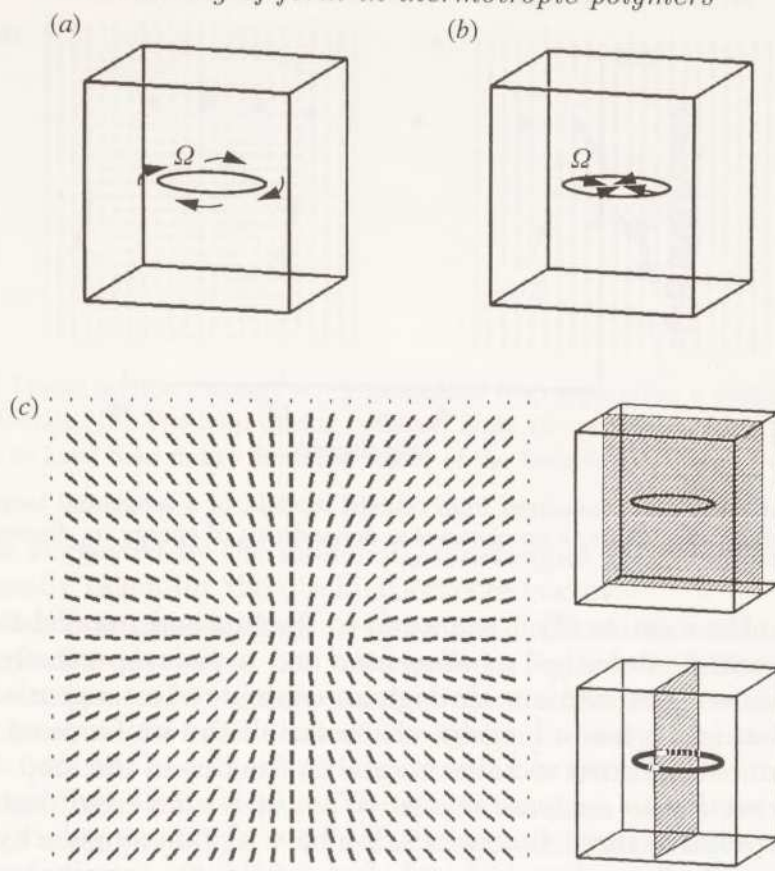
Figure 10. Limiting cases of $s = \pm\frac{1}{2}$ loops in which the rotation vector, Ω, maintains a constant angular relationship with the line as it curves around the loop. (a) Tangential loop with Ω parallel to the line. (b) Radial loop with Ω normal to the line and in the plane of the loop. (c) A diametric section through a tangential, $s = +\frac{1}{2}$ disclination loop. The director field will be identical for any such section, and the model corresponds exactly to the sections marked in the cubes. When the model was relaxed the loop did not move.

be one cell. It is scaled vertically to fit the model data. The relationships are comparable. It should be noted however, that the model loop was collapsing quite rapidly as the energy read-outs were taken, and thus it is difficult to be certain that the surrounding vector field represented a fully relaxed condition for any given loop diameter. For this reason we have refrained from any more detailed curve fitting which, in principle, could give a value for the effective core dimensions of the model; a matter which is addressed in more detail below. It should be noted that when a disclination loop is of sufficient radius to be visible in the light microscope, $R_l \gg r_c$, a value of 20 Å for r_c having been suggested (Cladis 1974).

5. Loops II (variable Ω class)

For disclinations in a elastic continuum it is possible to envisage loops in which the Ω vector maintains a constant angular relationship with the disclination line. Such loops are not possible for crystal dislocations, as the Burger's vector is a lattice vector and thus cannot take on a constantly varying orientation.

Two limiting cases of such loops are drawn in figure 10a, b. In (a) the Ω vector
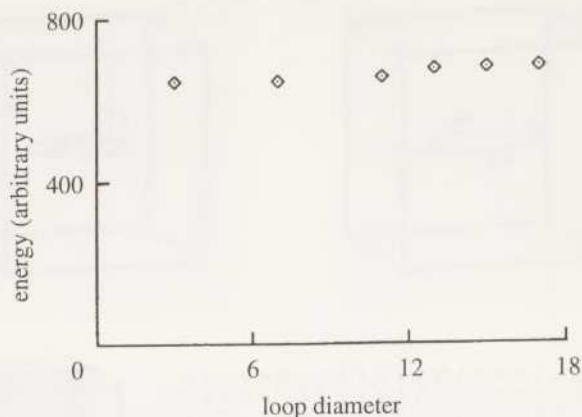
Figure 11. Plot of the energy, measured from relaxed models, of a tangential loop as a function of its diameter. There is no observable dependence of energy on diameter.

is tangential to the loop, in (*b*) it is normal to the line and parallel to the radius. The two loops will be described as *tangential* and *radial* respectively.

Figure 10*c* shows cross sections through an example of a tangential loop based on a disclination which has $+\frac{1}{2}$ wedge character all the way around. The model appears the same in all cross sections normal to the line of the loop. Imagine the loop shown in section to decrease in size. When it is small and central, the distortion field is radial in three dimensions. We have a point singularity of strength $+1$ at the centre of what is known as a *hedgehog* field, the terminology stemming from translations of Russian work (Volovik & Larentovich 1983). In his classification of point singularities, Poincaré (1886) described this type as a *nœud*. If the loop were to expand and grow out of the model, then the hedgehog would be converted to a monodomain with a resultant decrease in energy. It was observed, however, that, when the model was permitted to relax, the loop neither collapsed nor grew. The exception was when it was within one or two cells of the boundary of the model, in which case it was 'sucked out' by image forces to give a monodomain.

It is interesting to estimate the energy of such an arrangement as a function of the radius of the loop. Firstly, for a hedgehog point singularity, the energy of an element of material at radius r will scale as $1/r^2$, and thus the total energy of a shell of volume $4\pi r^2\,\mathrm{d}r$ will be independent of radius. Hence the total energy of a hedgehog field will be linearly dependant on its radius, R, in fact it is given as (Dubois-Violette & Parodi 1969):

$$E_{HH} = 8K\pi R.$$

Figure 11 is a plot of energy measured from relaxed models containing loops of different size. The energy of the model appears to be independent of the radius of the loop.

It is interesting to look at the implications of this finding. If it is assumed that the central sphere of material exactly girdled by the loop is essentially a monodomain set within the hedgehog, then the energy relaxed by the presence of a loop of radius, R_1, will be $8\pi K R_1$. This energy will be offset by the extra distortion energy, E_d, associated with the line of the disclination loop, that is $2\pi R_1 E$. Note that both energies scale linearly with R_1, but that for them to be
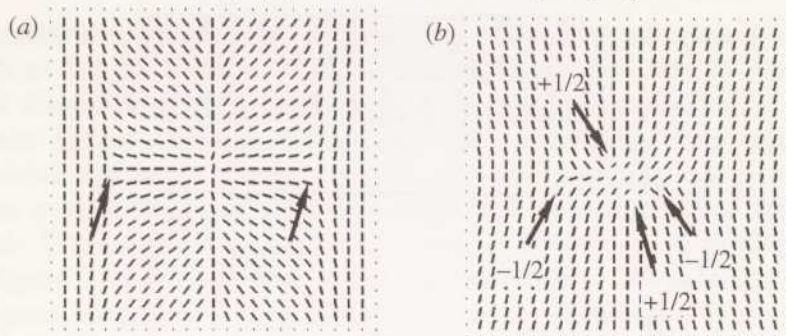
Figure 12. (*a*) Model section through a $-\frac{1}{2}$ tangential loop separating a central hedgehog field from a monodomain. (*b*) The loop during collapse. Note the presence of a $+\frac{1}{2}$ tangential loop which appears to have been drawn from the centre of the hedgehog by the encroaching $-\frac{1}{2}$ loop.

in balance as suggested by the model, E_d must equal $4K$, which is several times the value usually taken for the disclination core energy.

A tangential loop consisting of a $-\frac{1}{2}$ wedge disclination, would, if reduced to a point singularity, give what has been called a *hyperbolic hedgehog*. It is alternatively known as a *col* or saddle point (Poincaré 1886). As with the hedgehog its strength is equal to twice that of the tangential loop from which it can be generated; -1 in this case. Such an organization is not modelled further here.

Radial loops based on $+\frac{1}{2}$ or $-\frac{1}{2}$ twist disclinations would reduce to a point singularity, of strength $+1$ or -1 respectively, with essentially twist distortion. Radial loops and their related point singularities are not described further here.

Returning to a hedgehog field, it is possible to envisage such a point and its radial distortion field lying within a monodomain if it is surrounded by a tangential loop of strength $-\frac{1}{2}$. The starting structure is shown in figure 12*a*. When this arrangement is permitted to relax, the loop collapses eliminating the hedgehog. Figure 12*b* shows a later stage in the process. It is interesting that a $+\frac{1}{2}$ loop seems to have nucleated right at the centre and is drawn outwards towards the incoming $-\frac{1}{2}$ one, although not exactly in the same plane. The cancellation of the $+1$ point in this way can be seen as the result of the superposition of a -1 point which would extend outwards from the $-\frac{1}{2}$ loop if it were present by itself. In energy terms, the balance which meant that a $+\frac{1}{2}$ loop forming the core of a hedgehog would neither collapse or expand, at least in our model, does not pertain to the inverse situation of a $+1$ point surrounded by a $-\frac{1}{2}$ loop and thence a monodomain. In this case a reduction in loop radius will reduce the volume of material containing hedgehog distortion as well as the length of the $-\frac{1}{2}$ line. The collapse observed in the model is to be expected. A local hedgehog field can be associated with the presence of an impurity particle which provides homeotropic boundary conditions. It can be made compatible with a surrounding monodomain through association with an encircling $-\frac{1}{2}$ tangential loop. The force of attraction between the particle and loop has been calculated (Terentjev 1987).

6. Escape

Observations of the structure of nematic liquid crystals entrained in capillary tubes (Meyer 1973; Anisimov & Dzyaloshinskii 1972; Williams *et al.* 1972; Cladis
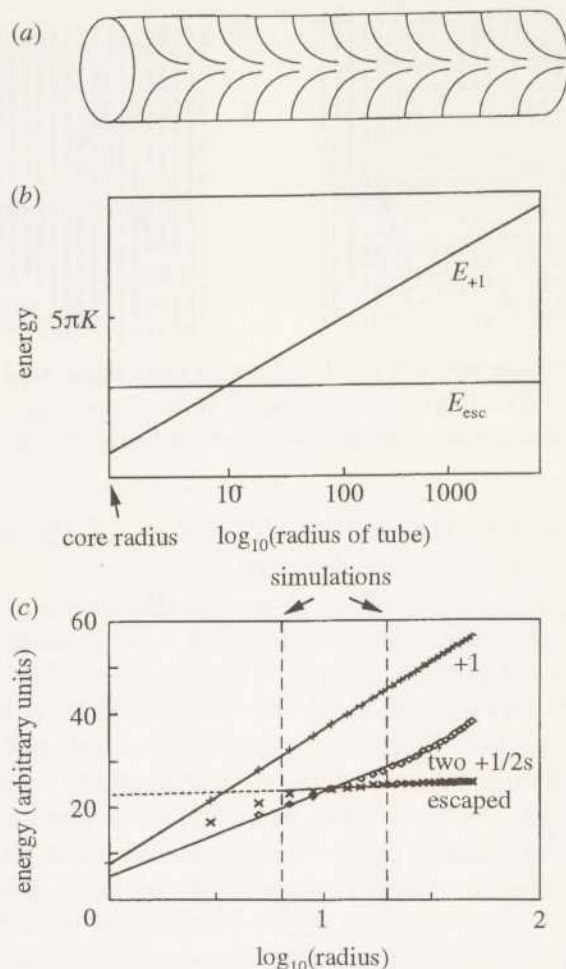
Figure 13. (a) Representation of the escaped configuration within a capillary tube treated to ensure homeotropic boundary conditions. (b) Plot of energies of: +1 disclination along the axis of a capillary calculated from $E_{+1} = \pi K(\ln(R/r_c) + 1)$ and of the escaped configuration from $E_{esc} = 3\pi K$ (Cladis 1974). (c) Model calculations of energies as a function of capillary radius, R, for the following configurations: +1 along axis; +1 dissociated into $2 + \frac{1}{2}$ axial lines; the escaped configuration. The vertical dashed lines correspond to model sizes for which relaxation sequences have been run.

& Kléman 1972) have underlined another aspect of the instability of disclinations of integral strength. Not only can they decompose into two halves, but they can escape into the third dimension which effectively eliminates any line singularity as illustrated in figure 13a. The capillary tube experiments have generally involved the treatment of the inside of the tube so as to ensure homeotropic boundary conditions which would tend to induce a +1 radial line along the axis of the tube. If this unstable line were actually to form, it would have two options. It could decompose into two halves which would repel each other towards the walls of the tube, or it could, terminated by half a hedgehog, escape from the nematic melt along the axial direction of the tube. Cladis (1974) has calculated (for equal elastic constants) that at a tube radius larger than 10 times the core radius of the disclination, the energy of the escaped configuration, which is independent of the tube radius, will be less than that of the original +1 line. The plots of these energy functions are shown in figure 13b. It can be argued that the core radius should

approach molecular dimensions, although for a +1 line (as opposed to a $\frac{1}{2}$ line) it is put as high as 0.2 μm (Cladis 1974). Cladis does not consider in equivalent detail the case of dissociation into two halves as a competing possibility. It is possible to model the different configurations and thus determine their relative energies. The +1 model was built exactly as such, the escaped and two $\frac{1}{2}$s configurations were set as a starting condition but permitted to relax before the energy was determined. The energies, in arbitrary units as a function of model diameter are shown in figure 13c. It should be noted that the values towards the left-hand side of the diagram correspond to models of no more than about four cells in radius, and thus should be treated with some circumspection. Hence, the extrapolation of the lines from larger model sizes are probably more reliable indicators of energies towards the left of the plot. At larger sizes of model there is a deviation of the energy plot for two $\frac{1}{2}$s towards the +1 line. This behaviour can be related to less than perfect relaxation of the large models within the computing time-frame available. Given these caveats, the model energies show a number of interesting features. The escaped energy, which as predicted, is independent of tube radius, crosses the +1 line at a model of radius four cells. Comparison with figure 13b would suggest that the model corresponds to a core diameter of approximately one cell. One would expect a value of this order and it was previously assumed for the calculated plot of figure 9. This result has important implication for the model in general in that it implies that it will only handle disclination core energies reliably when the cell size approximates to the core size, possibly in the region of 10 times molecular dimensions. It has already been argued that in this size range the model should include thermal fluctuations of the directors, and thus would not be totally appropriate for this reason. The conclusion is that the model, at size scales appropriate to the optical observation of texture, will underestimate disclination core energies, however, disclination processes which are dominated by the interaction of the long range distortion fields will still be accurately modelled. Figure 13c implies that the minimum energy configuration for the +1 line boundary conditions will be two axial half disclinations for tube radii up to approximately 30 times the core radius, and thereafter, the escaped structure. For all practicable tube radii, the minimum energy structure will be the escaped structure.

The model enables us to explore the development of escaped structures, and this has been done for the two radii indicated as vertical dashed lines on figure 13c, one for which the minimum energy structure would be two $\frac{1}{2}$ disclinations, the other, escape. Figure 14 shows that the final structure obtained from the model depends on the starting configuration. For +1 line (14a) and random (14b) starting conditions, the final structure after relaxation (14c) is that of two half disclination lines approximately parallel to the tube axis, the structure predicted to have the minimum energy for the tube diameter modelled. If the starting structure is an axial monodomain (14d), then the final structure is the escaped one which is metastable for this radius (14e). The implication of the model is that the final structure obtained is influenced by the starting conditions, a possibility already alluded to by those doing the capillary tube experiments (Williams *et al.* 1973), in that the filling of the tubes with a nematic liquid could induce axial flow alignment which might favour an escaped structure. It has been suggested by Friedel (1922) that the true homeotropy at the surfaces could be compromised by the field associated with capillary flow on filling. The issue of mechanism is also
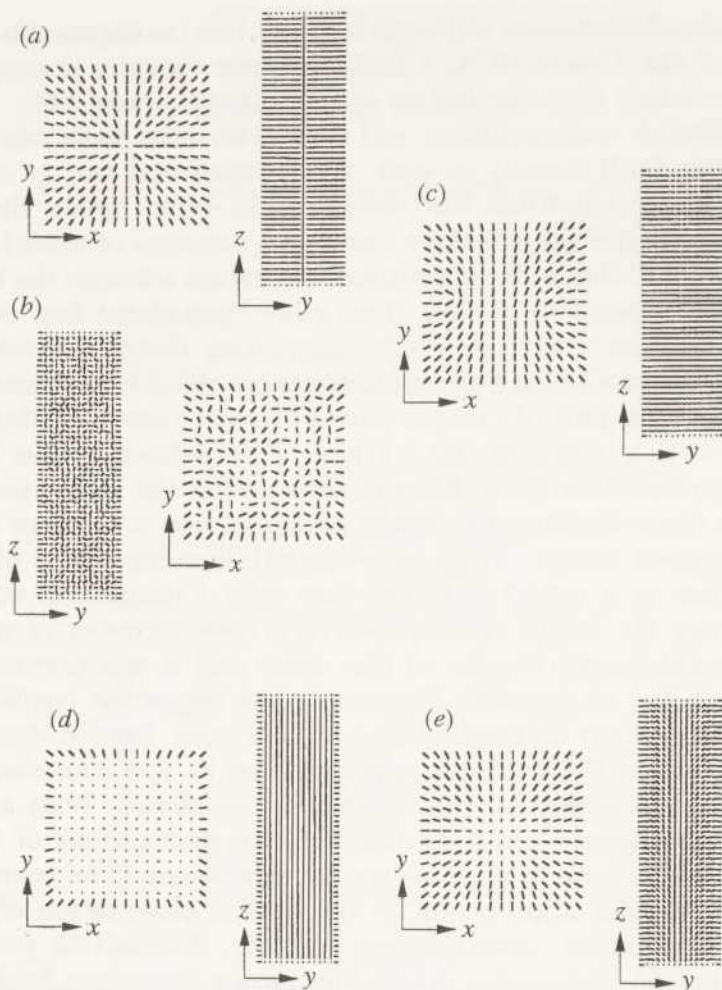
Figure 14. Sections through a model of a capillary tube with homeotropic boundary conditions. Even though a square section has been used in this model, the boundary conditions are normal to a circle of radius equal to half of the square edge. (*a*) Starting conditions set for a +1 disclination. (*b*) Random starting conditions (note fixed boundary settings) (*c*) Typical result of relaxation of models with starting conditions (*a*) or (*b*). The +1 disclination has decomposed into two +$\frac{1}{2}$s which have moved apart. (*d*) Starting conditions with a an axial monodomain. (*e*) Result of relaxation of model (*d*). The configuration has escaped.

highlighted in figure 15 which show structures obtained for a larger tube radius (identified on figure 13*c*). In figure 15*a* the starting condition was the +1 line, and the metastable structure seen after relaxation is that of two halves. However, for random starting conditions, there is escape even though this is far from perfect and the plan view of figure 15*b* shows four wedge disclinations, one of strength -$\frac{1}{2}$ and three of +$\frac{1}{2}$. It is possible that the modelling of yet larger radii, to give situations in which the escaped structure is the lowest energy by a significant factor will yield much better escaped structures. However, increased size, as ever, brings with it increased computational difficulties.

An integral disclination is inherently unstable with respect to both energy, as evidenced by dissociation into two half strength lines, and topology which provides the possibility of escape. The model observation that a +1 disclination will split into halves whether or not a escaped condition is overall of the lowest
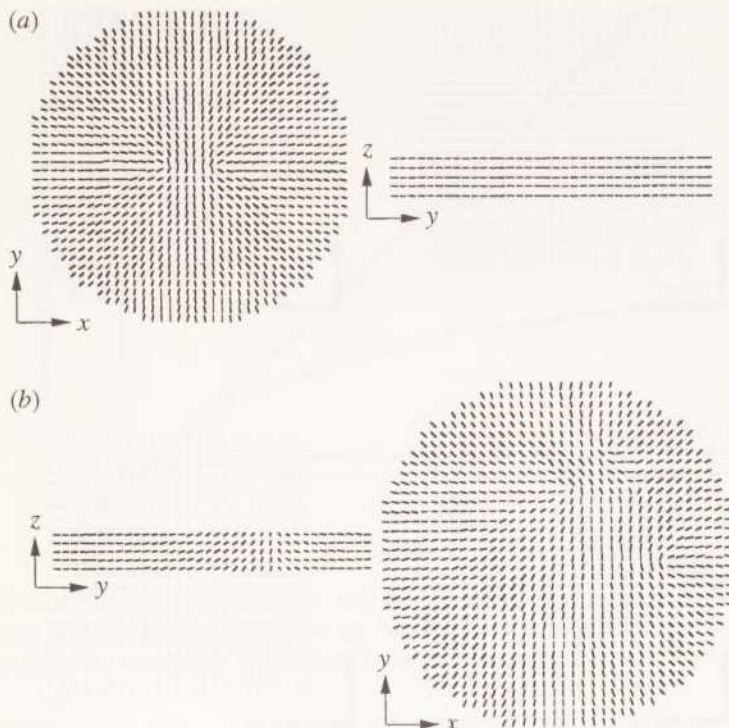
Figure 15. Relaxed models for capillary tubes of dimensions corresponding to the second (right-hand) vertical line on figure 13c. (a) Model started from an axial $s = +1$ disclination. (b) Random starting conditions.

energy, prompts observation of a $+1$ line included within the model and capped with two semi hedgehogs as shown in figure 16a, b. This line can be viewed as a $+\frac{1}{2}$ tangential loop compressed into a line. Once the model is permitted to relax, the line opens out into the loop, and sections such as figure 16c, d, show pairs of $+\frac{1}{2}$s. The loop reached an approximately circular shape very quickly, but then showed no tendency to change further in diameter or move out of the model. Escape would correspond to the loop being drawn out from the model by image forces, an occurrence which would require, at least, the loop to move from its symmetrical position. It is also a process requiring much longer range cooperative motion than the original decomposition of the $+1$ line into the loop. It would thus appear that, in mechanistic terms, a $+1$ line is able to express is energetic instability more readily than its topological instability.

There is ample experimental evidence that the direction of escape changes at intervals along the tube axis to give either $+1$ or -1 points along the tube axis. Such a structure was modelled in a previous paper using less fully developed algorithms, in which the orientational steps made in response to the local director field could be very large. We have been unable to repeat this result in the current work. It is also apparent from comments made in the experimental papers such as Cladis (1974), that these points are often seen to be associated with particles or small bubbles. It is possible that escaped structures within capillaries are facilitated by the presence of impurities which form point nuclei. Work to simulate the influence of such 'impurity' defects is in train.
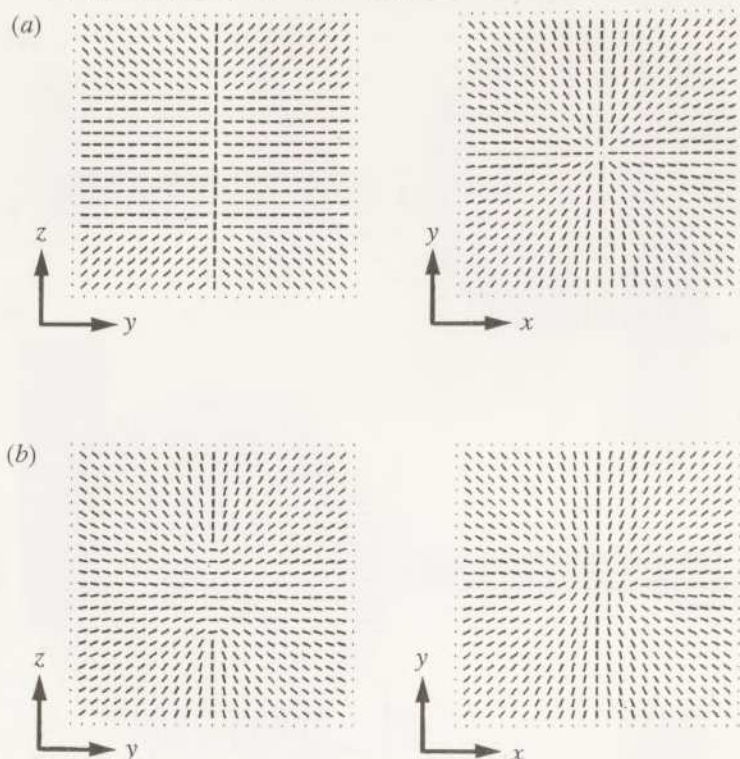
Figure 16. A model of a +1 line within radial (homeotropic) boundary conditions. The line is shorter than the height of the model along the Z axis, and is terminated by two semi hedgehogs. (*a*) Starting configuration with terminating regions only approximately modelled. (*b*) After relaxation for 164 iterations per cell. The hedgehog fields are clearly apparent, while the +1 line has opened up into a $+\frac{1}{2}$ tangential loop.

7. Liquid crystalline polymers: the case of unequal Frank constants

The adaptation of the model to treat the case of unequal constants has already been considered (Bedford & Windle 1993). Polymeric materials will tend to have a high splay constant in relation to twist and bend on account of the necessity of chain ends to compensate for the change in density with position which would otherwise be a feature of splay. For high molecular mass polymers where there is a paucity of chain ends, splay, if it is not compensated by equal and opposite distortion in an orthogonal plane, will require molecular diffusion to achieve the required density of ends in the region of highest splay distortion. Not only will there be kinetic limitations, but the special positioning of the ends will mean an entropic addition to the total energy. It should also be pointed out that if a nematic polymer molecule is capable of hairpin bends, perhaps where it contains short flexible sequences of units, then the hairpin can play the part of a chain end as far as density compensation in splay is concerned. Figure 17 shows the calculation of splay, twist and bend constants for a liquid crystalline polymer molecule of specific chemistry as a function of chain length. The constants were determined using the equations due to Odijk (1986) while the values of persistence length were determined by Monte Carlo molecular modelling procedures (Bedford *et al.* 1992). Both twist and bend constants depend on the persistence length which tends to a constant value for molecules of sufficient length, while the splay constant is linearly dependant on the contour length of the chain. The
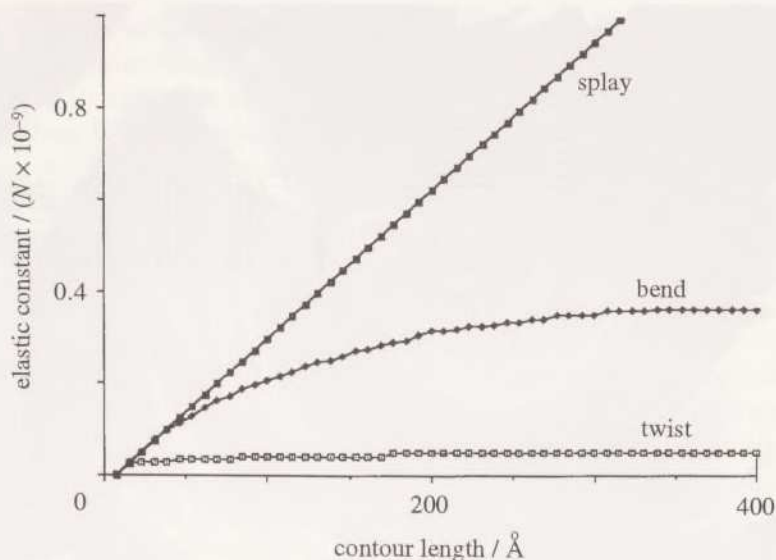
Figure 17. Calculations of the splay, twist and bend energies using the equations of Odijk (1986). The persistence lengths were determined by Monte Carlo modelling (Bedford *et al.* 1992) The molecule is a random copolymer of hydroxybenzoic and hydroxynaphthoic acids.
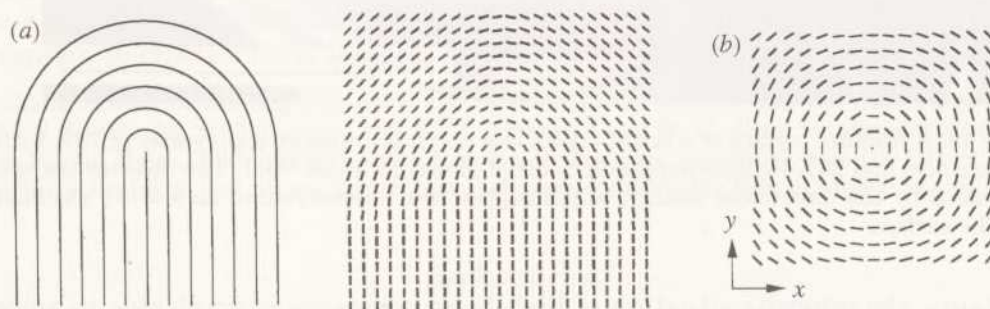

Figure 18. Director fields calculated with the splay energy set to 100 times that of bend or twist: (*a*) Around an $s = +\frac{1}{2}$ wedge disclination showing the 'archway' form. (*b*) Around an $s = +1$ line. Although the model was permitted to relax there was no tendency for the line to dissociate into $\frac{1}{2}$s. It can be viewed as the top part of two 'archways' face to face.

modifications of the director field around a disclination of strength $\frac{1}{2}$ as a result of unequal constants have already been well documented. The archway arrangement for the case of splay constant 100 times that of bend is shown in figure 18*a*. The distorted part of this field is equivalent to one half of a $+1$ disclination line with the directors arranged to give concentric circles. The implication being that, in this case, there would be no energy to be gained through the dissociation into two $\frac{1}{2}$s. Figure 18*b* is a fully relaxed model of such a $+1$ line for the splay constant set at 100 times that of both twist and bend. There is no evidence of dissociation. The significance of this fact is that it provides a rationale for explaining evidence for this type of $+1$ line, as opposed to the radial form, seen on fracture surfaces of liquid crystalline polymers such as that shown in figure 19. This is a polymer with chains of uniform stiffness which are unlikely to be able to form hairpin defects within the mesophase.

While main-chain liquid crystalline polymers are likely to exhibit high splay
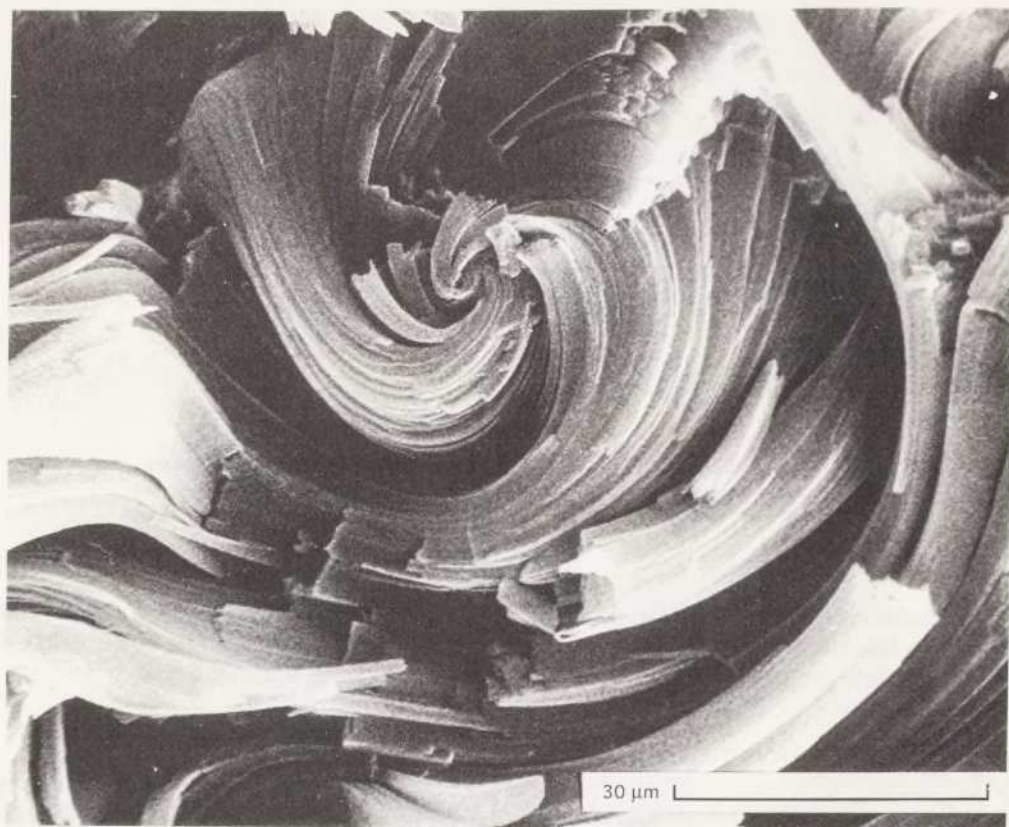
Figure 19. A fracture surface of a liquid crystalline polymer (random copolyester of 75% hydrox-ybenzoic acid and 25% hydroxynaphthoic acid) of molecular mass 5000. The director trajectory, as revealed by the directional fissility, would suggest the intersection of an $s = +1$ disclination with the surface.

constants, the opposite situation of high bend constants is applicable to smectic liquid crystals where the resistance to splay deformation between the smectic layers effectively limits bending along the molecular axis. There is a report (Cladis 1974) for a smectic phase of an unescaped $+1$ disclination line along the axis of a capillary tube treated to obtain homeotropic boundary conditions. What is more, on heating into the nematic, the $+1$ was observed to split into two $\frac{1}{2}$s, arranged as a double helix; there was no escape. It was further noted that the only conditions under which escape could be initiated on heating into the nematic phase were those in which second phase particles were present to nucleate point singularities.

8. Conclusions

The major focus of this work has been the development of a lattice model for the dynamic simulation of disclination processes in liquid crystalline phases. In applying it to recognized phenomena, many of which have been studied experi-mentally and treated theoretically in the past, we continue to gain confidence in it as a new tool.

The modelling has emphasized the fundamental importance of disclination lines of strength $\pm\frac{1}{2}$. Whereas loops defined by a single rotation vector, Ω, will be the means of propagation or annihilation of rotational distortion, loops in which the

Ω vector follows the curvature of the line lead to director fields which assume the characteristic of a point singularity as the loop approaches zero radius. Modelling has shown that, in the size range treated, the energy of a $+\frac{1}{2}$ tangential loop within a hedgehog field, is independent of its radius.

Modelling a $+1$ line, such as may be envisaged at the centre of a homeotropically treated capillary, has demonstrated that it will decompose into two $+\frac{1}{2}$ strength lines, even at a capillary radii where the escaped configuration is of lowest energy. In mechanistic terms, the decomposition of a $+1$ line as a result of its energetic instability occurs more readily than escape due to its topological instability, which is thus hindered.

The calculation of model energies for the several underlying configurations associated with topological instability of a unit strength line in a capillary tube, demonstrates that the model will handle core energy exactly when the scale is such that the core diameter is equivalent to one unit cell, although thermal fluctuations will not then be negligible.

The work draws attention again to the possibility that an essential role is played by impurity particles in establishing escaped structures in capillaries.

The application of the model to situations in which the splay constant is much higher than either bend or twist, enables microstructures typical of main-chain liquid crystalline polymers to be simulated. In particular, the model observation that a $+1$ line based on bend distortion is no longer energetically unstable, is able to explain microstructural features seen in thermotropic random copolyesters.

References

Anisimov, S. I. & Dzyaloshinskii, I. E. 1972 A new type of disclination in liquid crystals and the stability of disclinations of various types. *Soviet Phys. JETP* **36**, 774–779.

Assender, H. E. & Windle, A. H. 1994 A two dimensional lattice model of disclinations in liquid crystals: the choice of energy function. *Macromolecules*. (In the press.)

Bedford, S. E., Nicholson, T. M. & Windle, A. H. 1991 A supra-molecular approach to modelling of textures in liquid crystals. *Liquid Crystals* **10**, 63–71.

Bedford, S. E., Yu, K. & Windle, A. H. 1992 Influence of chain flexibility on polymer mesogenicity. *J. chem. Soc. Faraday Trans.* **88**, 1765–1773.

Bedford, S. E. & Windle, A. H. 1993 Modelling of microstructure in mesophases. *Liquid Crystals* **15**, 31–63.

Bouligand, Y., Cladis, P. E., Liébert, L. & Strzelecki, L. 1973 *Mol. Cryst. Liq. Cryst.* **21**, 1.

Cladis, P. E. & Kléman, M. 1972 Non-singular disclinations of strength $S = +1$ in nematics. *J. de Phys.* **33**, 591–598.

Cladis, P. E. 1974 Study of the nematic and smectic A phases of N-p-cyanobenzylidene-p-n-octyloxyaniline in tubes. *Phil. Mag.* **29**, 641–663.

Dubois-Violette, E. & Parodi, O. 1969 Émulsions nématiques effets de champ magnetiques et effets piezoélectriques. *J. Phys. Paris* **30**, 4–57.

Frank, F. C. 1958 On the theory of liquid crystals. *Discuss. Faraday Soc.* **25**, 19–28.

Friedel, G. 1922 Les etats mésimorphes de la matière. *Ann. Phys.* **18**, 273–474.

Hanna, S., Lemmon, T. J., Spontak, R. J. & Windle, A. H. 1992 Dimensions of crystallites in a thermotropic random copolyester. *Polymer* **33**, 3–10.

Kilian, A. & Hess, S. 1989 Derivation and application of an algorithm for the numerical calculation of the local orientation of nematic liquid crystals. *Z. Naturf.* **44a**, 693–703.

Kilian, A. & Hess, S. 1990 On the simulation of the director field of a nematic liquid crystal. *Liquid Crystals* **8**, 465–472.

Kléman, M. 1983 *Points, lines and walls.* Chichester: Wiley.

Lebwohl, P. A. & Lasher, G. 1972 Nematic-liquid-crystal order – a Monte Carlo calculation. *Phys. Rev.* A **6**, 426–429.

Lehmann, O. 1904 *Flüssige Kristalle.* Leipzig: Engelmann.

Meyer, R. B. 1973 On the existence of even indexed disclinations in nematic liquid crystals. *Phil. Mag.* **27**, 405–424.

Odijk, T. 1986 Elastic constants of nematic solutions of rod-like and semi-flexible polymers. *Liquid Cryst.* **1**, 553–559.

Poincaré, H. 1886 Sur les courbes définies par les équations differentielles. *J. de Math.* **2**, 151–217.

Spontak, R. J. & Windle, A. H. 1990 Electron microscopy of non-periodic layer crystallites in thermotropic random copolymers. *J. Mater. Sci.* **25**, 2727–2736.

Terentjev, E. M. 1987 Moment theory of elasticity and interaction of disclinations in liquid crystals. *Sov. Phys. Crystallogr.* **32**, 166–171.

Volovik, G. E. & Larentovich, O. D. 1983 *Sov. Phys. JETP* **58**, 1159.

Williams, C., Pieranski, P. & Cladis, P. E. 1972 Nonsingular $S = +1$ screw disclination lines in nematics. *Phys. Rev. Lett.* **29**, 90–92.

Williams, C., Cladis, P. E. & Kléman, M. 1973 Screw disclinations in nematic samples with cylindrical symmetry. *Mol. Cryst. Liq. Cryst.* **21**, 355–373.

Zocher, H. & Birstein, V. 1929 Beträge zur Kenntnis der Mesophasen. *Z. Phys. Chem.* A **142**, 113–125.

Discussion

A. DONALD (*Cavendish Laboratory, University of Cambridge, U.K.*). Is it possible to compare your models with experiment and hence extract the relative values of the elastic constraints.

A. H. WINDLE. In principle yes. Although this paper concentrates on the modelling aspects, it is clear that there are many features of the observed microstructures of liquid crystalline polymers which are not seen in small molecule mesophases. The modelling so far would indicate that some of these features, namely the fissile nature of structures produced by shear, and the absence of hedgehog type features in the quiescent microstructures, would suggest the presence of a high splay constant. Work to measure the trajectories around $\frac{1}{2}$ disclination is in progress.

T. C. B. MCLEISH (*University of Leeds, U.K.*). The simulation on the dislocation you called the hedgehog loop seemed to show that these possessed a stability independent of their size. This would be surprising from a theoretical point of view if the stability were due to the cancellation of a repulsive and an attractive term in the total energy for the loop, as these have different dependencies on the size of the loop. For example, the core energy would be linear in the size of the loop, while the far field Frank terms would be logarithmic. Is it perhaps the case that the approach to equilibrium is in this case much slower than the timescale of your simulations?

A. H. WINDLE. We are sure that the apparent stability of a hedgehog loop is not an artifact of the model. Wedge-twist loops collapse to a monodomain very rapidly, and a hedgehog loop written in too close to the boundaries of the model rapidly expands outwards under the influence of image forces to leave behind a perfect monodomain. The primary difference between the wedge-twist loop and the hedgehog one is that if the former were to be induced to expand, then the line energy would increase with radius with an additional log term dependant on the extent of the long range elastic field. In line with simple dislocation theory, one might take the extent of the elastic distortion to be equal to the radius of the loop. Such a loop will minimize its energy by shrinking, and self annihilating. On the other hand, the expanding hedgehog loop girdles volume, which approximates to a monodomain, hence its expansion can be seen as the elimination of the hedgehog. Correspondingly, it is not obvious in this case how, if at all, the range of the elastic distortion (that which influences the log term) would vary with loop radius. The fact that both the recovered energy from the hedgehog to monodomain conversion, and the total core energy of the dislocation line, are primarily dependant on the loop radius may point to a balance of energies. However, a loop energy independant of radius implies that the energy of the disclination line is of the order of $4K$, where K is the Frank elastic constant. It is interesting to speculate that a $-\frac{1}{2}$ wedge Class II loop, should collapse to form a hyperbolic hedgehog of its own accord, as the energy of this point defect is 33% of the hedgehog (J.R. Hobdell, personal communications) on account of splay–splay compensation.

With respect to the experimental observation of the collapse of Class II loops into points; it is worth nothing that points may well be associated, indeed stabilized by, second phase particles, and that in any case the hedgehog is the highest energy point, for a given radius, even in the case of equal elastic contants.

E. L. THOMAS (*MIT, Cambridge, U.S.A.*). We have shown (S. Hudson *et al.*, *Macromolecules* **26**, 1270 (1993)) that it is possible to measure the Frank elastic contants from the variation of the director field about an isolated disclination using the lamellar decoration technique. Interestingly, if one measures the radial dependence of the variation of the director field, below distances of around 0.1 mm from the disclination the measured apparent elastic anisotropy begins to depend on the radial distance from the defect core. This effect could be due to either a breakdown in Frank theory, since the distortions are growing as 1/4, and/or a real material property effect due to variability of the liquid crystalline material near the defect core, such as segregation of low molecular mass material and/or hairpins to alleviate the distortions. If heterogenieties in the LC material are the source of the variation of the apparent elastic anisotropy, then an effect analogous to the 'Cottrell-atmosphere' in a metal system, whereby impurity atoms are attracted to dislocation core and influence subsequent dislocation motion, may occur. G. Mazelet & M. Kléman (*Polymer* **27**, 714 (1986)) have previously commented on the different mobilities of $S = +\frac{1}{2}$ and $S = -\frac{1}{2}$ disclinations in a thermotropic LC polyester which could arise from such heterogeneities.

A. H. WINDLE. The observation that the apparent elastic anisotropy around a disclination changes as the core is approached is especially intriguing. As with dislocations, the whole issue of core structure and energy is fraught with difficulties. It may be that at a finite temperature the quality of director alignment with

its immediate neighbourhood is lower, or put a different way that the nematic to isotropic transition temperature is lowered where the distortion is significant. The most effective driving force for the formation of Cottrell atmospheres would be splay distortion associated with polymers. Is it possible to relate the observed change in anisotropy near to the core with a reduction in the splay component of distortion? In the example of a high splay constant polymer, one might expect to show up as a reduction in the archway character of a $+\frac{1}{2}$ line defect.

E. L. THOMAS. If the crystalline lamellae that grow and serve to decorate the underlying glassy nematic texture are held for long times at temperatures just below the T_m, the significant reorganization of the nematic texture by crystallization does indeed occur, prohibiting valid observations of the director field. Thus one needs to use a deep-quench to nucleate cystals massively so that the resulting small crystals effectively decorate without major perturbation to the glassy nematic phase from which they grow. Another key variable in the use of lamellar decoration is the influence of temperature dependence of the order parameter which controls the temperature dependence of the elastic constants. Therefore, we are currently attempting to quench samples from various temperatures in the nematic phase régime, in the hope that since thermal diffusivity greatly exceeds mass diffusivity, appropriate rapid quenching may be able to reflect the temperature dependence of the disclination near-core structure.

A. H. WINDLE. The crystallization that occurs in thermotropic random copolyesters raises many issues, most of which are beyond the scope of this paper. However, the degree to which the director field may be modified by the formation of crystallites during cooling is pertinent to any comparison between modelling and experiment. The first-order answer is that the crystallization appears to decorate rather than 'rewrite' the nematic microstructure. Crystallites in the region of a boundary of a thin layer of the polymer, where the director field is changing most rapidly, are themselves curved. It is not possible to say that the crystals have no influence on the director field, but if it is present it is distinctly a second order effect. Furthermore we have not been able to detect any difference in director microstructure between quenched samples and those which have been annealed for several hours whithin a few degrees of the melting point, although in the latter case the crystals themselves are better formed. However, the extremely rapid formation of crystals which do require some degree of longitudinal sorting of the random chains for their order, does seem surprising. Recent diffraction studies (S. Hanna *et al.*, *Nature, Lond.* **366**, 546 (Dec 1993)) show that the segregation is present in the melt, which thus contains regions which should possibly be classified as smectic rather than nematic. Crystallization, as indicated by the solidification of the polymer, a thermal transition, and the development of sharp interchain X-ray peaks, represents the development of lateral order within the regions within which the chains were already longitudinally matched in the melt. It is possible therefore that these presegregated regions have their own influence on the director microstructure via the relative values of the splay, twist and bend constants.